Infrared phonon modes in multiferroic single-crystal FeTe_{2}O_{5}Br

K. H. Miller, X. S. Xu, H. Berger, V. Craciun, Xiaoxiang Xi, C. Martin, G. L. Carr, and D. B. Tanner

Phys. Rev. B **87**, 224108 — Published 17 June 2013

DOI: 10.1103/PhysRevB.87.224108

Infrared phonon modes in multiferroic single-crystal $FeTe_2O_5Br$

K. H. Miller,[1] X. S. Xu,[2] H. Berger,[3] V. Craciun,[4] Xiaoxiang Xi,[1] C. Martin,[1] G. L. Carr,[5] and D. B. Tanner[1]

[1] *Department of Physics, University of Florida, Gainesville, Florida 32611-8440, USA*
[2] *Materials Science and Technology Division, Oak Ridge National Laboratory, Oak Ridge, Tennessee 37831, USA*
[3] *Institute of Physics of Complex Matter, Ecole Polytechnique Federal de Lausanne, CH-1015 Lausanne, Switzerland*
[4] *Laser Department, National Institute for Lasers, Plasma, and Radiation Physics, Magurele, Romania*
[5] *Photon Sciences, Brookhaven National Laboratory, Upton, New York 11973, USA*

Reflection and transmission as a function of temperature (7[5]–300 K) have been measured on single crystals of the multiferroic compound $FeTe_2O_5Br$ utilizing light spanning from the far infrared to the visible. The complex dielectric function and other optical properties were obtained via Kramers-Kronig analysis and by fits to a Drude-Lortentz model. Analysis of the anisotropic excitation spectra via Drude-Lorentz fitting and lattice dynamical calculations have lead to the observation of 43 of the 53 modes predicted along the b axis of the monoclinic cell. The phonon response parallel to the a and c axes are also presented. Assignments to groups (clusters) of phonons have been made and trends within them are discussed in light of our calculated displacement patterns.

I. INTRODUCTION

Recently, significant attention has been given to a class of multiferroics in which specific magnetic ordering breaks inversion symmetry, thus allowing spontaneous polarization to arise.[1,2] This magnetically driven ferroelectric response is the most direct form of magnetoelectric coupling and is associated with large magnetoelectric[3] and magnetocapicative[4] responses. Electric dipoles induced by the ordering of magnetic dipoles remain highly susceptible to applied magnetic fields, thus making this class of multiferroics of interest from a technological point of view.[5] Recent studies on materials such as $TbMnO_3$,[6] $RbFe(MoO_4)_2$,[7] and $CoCrO_4$[8] all show the appearance of spontaneous polarization due to non-collinear magnetic ordering via spin-orbit mechanisms, viz., the standard spin-current and inverse Dzyaloshinski-Moriya models. A technological shortcoming of magnetically driven ferroelectrics possessing non-collinear magnetic moments has been the small value of induced spontaneous electric polarization observed. Much larger spontaneous polarizations have been predicted in materials where ferroelectricity arises from collinear magnetic ordering of spins.[9,10] In collinear magnetic ordering, moments may vary in amplitude but do not vary in direction; therefore, one does not expect the aforementioned spin-orbit-related interactions to be important,[11] enabling the much stronger exchange striction interaction as the mechanism by which ferroelectricity is induced.

In this paper, we report our infrared studies on single crystals of the multiferroic $FeTe_2O_5Br$ compound, a magnetically driven ferroelectric with nearly-collinear incommensurate spin order. A previous study by Pregelj *et al.*[12] has reported significant changes in the magnetic and electric orders when external magnetic fields are applied along the different crystallographic directions. Strikingly, for $B \| b$ they observed that fields greater than 4.5 T destroyed the electric polarization completely. In our investigation of magnetoelectric coupling we measured transmission in the far-infrared down to 15 cm^{-1} (2 meV) and in external magnetic fields up to 10 T oriented along all three crystallographic axes. The significant magnetoelectric coupling previously shown by the application of external magnetic fields did not surface in our data. Here, we present a comprehensive report of the excitation spectrum in single crystal $FeTe_2O_5Br$. The modeling of the infrared active phonons as well as lattice dynamical calculations have lead us to make an interesting comparison to a previous infrared study on a similar geometrically frustrated spin-cluster oxyhalide compound, $FeTe_2O_5Cl$,[13] where an equal number of modes was predicted but a significantly lower number was reported.

Becker *et al.*[14] solved the crystal structure using single-crystal x-ray diffraction. The $FeTe_2O_5Br$ compound crystallizes in a layered structure where the individual layers comprise the *bc* plane in the monoclinic system ($P2_1/c$). The layers are weakly connected via van der Waals forces and slip at an 18° angle as they stack along the normal to the *bc* plane, thus defining the monoclinc *a* axis. A single layer is composed of $[Fe_4O_{16}]$ groups confined on top and bottom by $[Te_4O_{10}Br_2]$ groups. The three groups contain 16 common oxygens which connect them and also serve to create charge neutrality in the layers. The $[Fe_4O_{16}]$ groups consist of four edge-sharing $[FeO_6]$ distorted octrahedra. All iron ions possess a +3 oxidation state. More detailed descriptions of the crystal structure are found elsewhere.[14]

The $FeTe_2O_5Br$ compound exhibits nearly-collinear (7° of canting between the Fe1 and Fe2 sites) incommensurate antiferromagnetic ordering of its moments below T_N = 10.6 K.[15,16] The amplitude-modulated magnetic order is described with the wave vector $\mathbf{q}$=(1/2,0.463,0). Simultaneously, a ferroelectric polarization is induced perpendicular to $\mathbf{q}$ and the Fe^{3+} moments.[15] The ferroelectric order is attributed to the highly polarizable Te^{4+} lone pair electrons. Single-crystal x-ray diffraction measurements in the ordered state did not detect any change in crystal symmetry from the high temperature phase; however, clearly distinguishable changes in Fe-Te and Fe-O interatomic distances were observed that signified exchange striction as the means by which the inversion center is removed, thus allowing for ferroelectricity to arise.[16] Exchange striction is the mechanism by which magnetic ions shift away from their centrosymmetric positions to maximize their exchange interaction energies.[5,6]

II. EXPERIMENTAL PROCEDURES

Single crystals of $FeTe_2O_5Br$ were grown by standard chemical vapor phase method. Mixtures of analytical grade purity Fe_2O_3, TeO_2 and $FeBr_3$ powder in molar ratio 1:6:1 were sealed in the quartz tubes with electronic grade HBr as the transport gas for the crystal growth. The ampoules were then placed horizontally into a tubular two-zone furnace and heated very slowly by 50°C/h to 500°C. The optimum temperatures at the source and deposition zones for the growth of single crystals are 500°C and 440°C, respectively. After six weeks, many dark yellow, almost orange $FeTe_2O_5Br$ crystals with a maximum size of $8 \times 12 \times 1$ mm^3 were obtained. The powder x-ray diffraction pattern, obtained by using a Rigaku x-ray diffractometer, shows the monoclinic space group $P2_1/c$ for all $FeTe_2O_5Br$ crystals.

The zero-field, temperature-dependent (7–300 K) reflectance and transmittance measurements were performed on a $1.3 \times 8 \times 6$ mm^3 single crystal (crystal 1) using a Bruker 113v Fourier transform interferometer in conjunction with a 4.2 K silicon bolometer detector in the spectral range 25–700 cm^{-1} and a 300 K DTGS detector from 700–7000 cm^{-1}. The crystal was cooled using a flow cryostat. Room temperature measurements from 7000–33000 cm^{-1} were obtained

with a Zeiss microscope photometer. Appropriate polarizers were employed to span the desired spectral range.

Field-dependent (0–10 T) and temperature-dependent (5–300 K) transmission measurements in the far infrared were performed on a $0.3 \times 8 \times 5$ mm^3 single crystal (crystal 2) at beam line U4IR of the National Synchrotron Light Source, Brookhaven National Laboratory. The measurements employed a Bruker IFS 66-v/S spectrometer in conjunction with a 10 T Oxford superconducting magnet and a 1.8 K silicon bolometer detector. The spectral resolution was 0.25 cm^{-1}. A free-standing wire grid polarizer was oriented along the preferential polarization direction of the synchrotron beam.

At this point it is important to establish with confidence that we cooled our single crystal below 10 K in both the Oxford superconducting magnet and the Janis flow cryostat. The superconducting magnet is equipped with a variable temperature insert that cools in liquid He vapors. This same system has been used to accurately measure the properties of superconducting materials down to 2 K.[17] The accuracy of the cooling capacity of the flow cryostat was corroborated by comparing ratios of $\mathcal{T}_s/\mathcal{T}_n$ for the superconductor $Nb_{0.5}Ti_{0.5}N$ with those same ratios measured in the superconducting magnet. With the superconductor fastened to the cold finger of our flow cryostat with a copper clamp, the measured temperatures, below 10 K, agreed to within ± 1 K.

In materials where the crystal symmetry is orthorhombic or higher, the dielectric tensor can be diagonalized by a set of orthogonal principal dielectric axes that coincide with the three orthogonal crystallographic axes. For a monoclinic system, the crystallographic b axis is unique because it is perpendicular to both the a and c axes. Accordingly, a principal dielectric axis of the system is fixed along the crystallographic b axis. The other two principal axes lie in the ac plane, and their directions can change as a function of frequency. To fully resolve all IR-active modes in the ac plane of a monoclinic system a special three-polarization measurement technique is typically employed.[18] The aforementioned measurement technique requires specular reflection from a pristine ac plane of the crystal. Consequently, we performed single crystal x-ray diffraction on crystal 1 to see how the orthogonal crystallographic directions fell in relation to the crystal facets. A pristine ac plane for optical measurement was not available. Subsequent attempts to polish the layered material to achieve a measureable ac plane were not successful.

We measured the polarized reflectance on the bc face (as shown in the inset to Fig. 1) for field along b (a principal axis) and c (perpendicular to b). We measured the reflectance on the ab face for field along a (perpendicular to b) and also along b again. (Note that the a and c axes form an angle of 108° to each other.) The response of the $FeTe_2O_5Br$ along the principal b axis was identical as measured from both the bc and ab faces.

X-ray diffraction measurements were collected at 300 K on a four-circle Panalytical X'Pert MRD in a parallel beam geometry with Kα radiation. A θ–2θ scan was used to check that the sample surface corresponded to the bc plane while pole figure measurements were performed to find the spatial orientation of the a axis with respect to the bc plane.

III. RESULTS AND ANALYSIS

A. X-Ray diffraction

The XRD patterns acquired from the sample with the surface aligned perpendicular to the diffraction plane are displayed in Fig. 1. Only very narrow (h00) diffraction lines were observed, confirming that the sample was a high quality single crystal, with the surface aligned parallel to the bc plane. Several acquired pole figures helped identify the orientation of the a axis with respect to the bc plane. The inset to Fig. 1 contains the results of our XRD investigation, namely, a sketch of crystal 1 with the crystallographic axes (a, b, and c) superimposed on the crystal facets.

B. Reflectance and Transmittance Spectrum

The temperature-dependent reflectance spectra of $FeTe_2O_5Br$ for electric field oriented parallel to the a, b, and c axes in the frequency interval 30–1000 cm^{-1} (4–120 meV) is shown in Fig. 2. A strong sharpening of many modes accompanied by a hardening of resonance frequencies is observed with decreasing temperature. No drastic deviations from the room-temperature spectrum were observed along any of the three directions when cooling to 7 K. Particular attention was given to the excitation spectrum slightly above and below the 10.6 K multiferroic ordering temperature. The absence of anomalies in the spectra upon cooling below 10.6 K gives strong support to the observation of no crystal symmetry change in the ordered state; however, a subtle contradiction exists.[15] The high temperature $P2_1/c$ space group is centrosymmetric, but ferroelectricity, for which non centrosymmetry is a strict requirement, is observed below T_N. This in turn suggests that new infrared modes should accompany the transition. However, the small value of polarization measured (8.5 μC/m^2) leads one to suspect that these modes have small oscillator strengths.

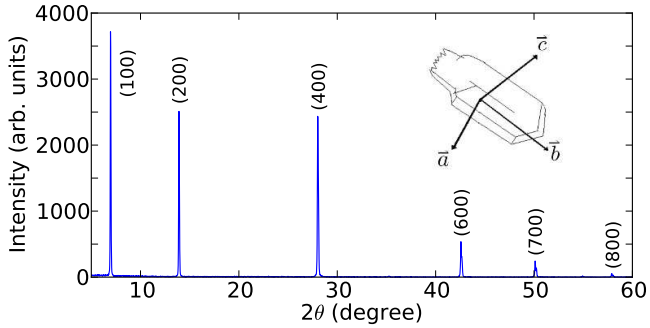

FIG. 1. The XRD pattern for the sample surface aligned perpendicular to the diffraction plane. The inset depicts the orientation of the crystallographic axes with respect to the facets of crystal 1.

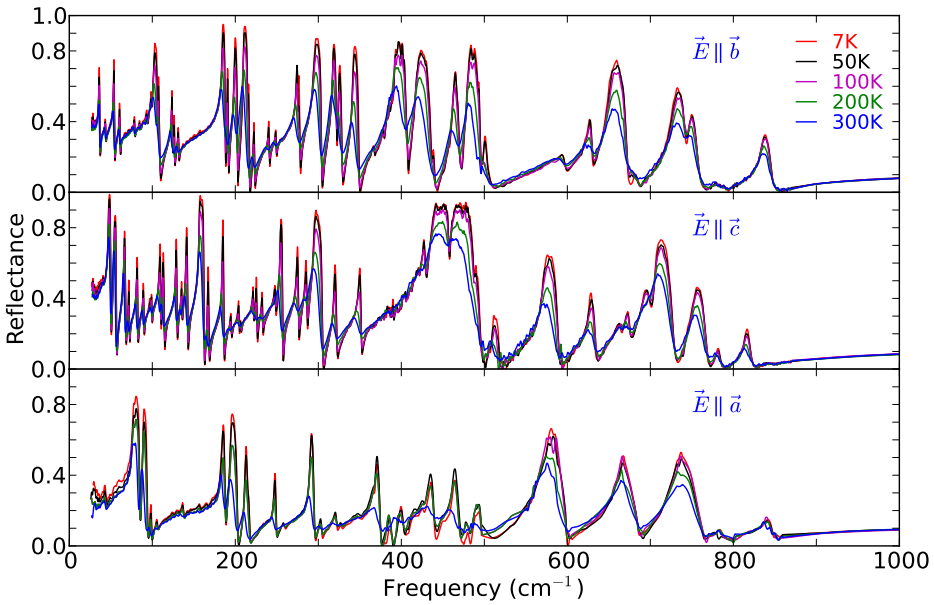

FIG. 2. (Color online) Temperature-dependent reflectance spectra of $FeTe_2O_5Br$ parallel to the a, b, and c axes.

Crystal 1 exhibits transmission at frequencies above the infrared phonon modes and below the absorption edge. The dimensions of the crystal only allowed for transmission with light polarized parallel to the b and c axes. As shown in Fig. 3, a sharp dip at 1850 cm^{-1} as well as a broad absorption centered at 3250 cm^{-1} are present along both polarizations. These anisotropic absorptions in the mid-infrared have been tentatively assigned to the vibrational bands of water that has been absorbed by the crystal (a likely occurrence during growth).

C. Field-dependent transmittance

Crystal 2 transmits at frequencies below the strong infrared phonons, in the gaps in-between the phonons, and in the mid infrared between the highest phonon and the onset of interband transitions. Particular attention was given to the transmission below the strong infrared phonons. No appreciable change in the spectra were observed for transmittance at 5 K measured parallel to the b and c axes with magnetic fields of 10 T applied along all three crystallographic directions. A class of low energy magnetic excitations called antiferromagnetic resonance modes (AFMR) are predicted to exist at finite frequencies in zero field and shift upon the application of external fields. AFMR modes in the $FeTe_2O_5Br$ have been reported in a recent electron spin resonance study below 400 GHz ($\sim$13 cm^{-1}).[20] However, in an external field of 10 T the modes remain slightly below the low frequency limit of our measurements.

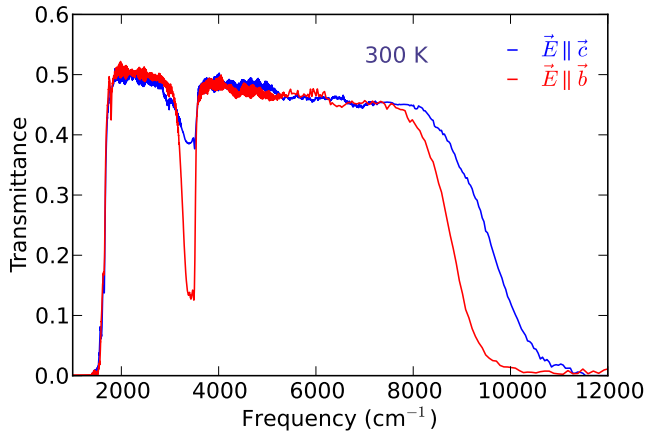

FIG. 3. (Color online) Transmittance of crystal 1 in the mid-infrared and near-infrared regions.

D. Determination of optical properties

We have used the measured reflectance and transmittance spectra of crystal 1 to extract the complex dielectric function. Because Kramers-Kronig analysis requires a single-bounce reflectance spectrum over a broad frequency region, we must first correct the measured reflectance spectra in regions where the crystal transmits by using a combined reflection and transmission analysis. An attempt to solve for the single bounce reflectance by inverting the full reflection and transmission equations leads to a transcendental equation with infinitely many solutions. Nevertheless, using the method employed by Zibold *et al.*,[21] i.e., assuming that k is small in the region of interest, leads to an approximation of reflection and transmission that can be solved numerically for a single solution.

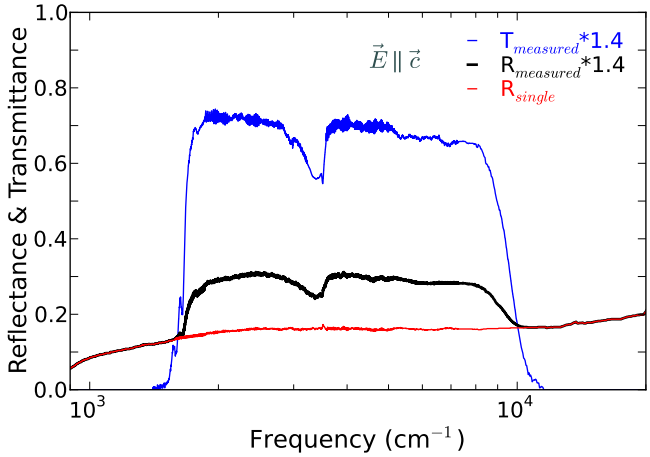

FIG. 4. (Color online) Single-bounce reflectance (red) as approximated from the scaled measured reflectance (black) and the scaled measured transmittance (blue) of crystal 1. The elevated level of measured reflectance throughout the transmission interval is expected due to additional light reflected from the back surface of the crystal.

The measured reflectance (not shown) and transmittance (Fig. 3) in the frequency interval 1500–10000 cm^{-1} were significantly lower than expected throughout this region of low absorption (Fig. 5). First, we expect $\mathcal{R}(\omega) + \mathcal{T}(\omega) = 1$, but we measure $\mathcal{R}(\omega) + \mathcal{T}(\omega) = 0.6$. Note that the reflectance is expected to include light reflecting from both the front and back surfaces of the crystal, including, multiple internal reflections. The low measured values were attributed to the scattering of light from facets existing on the back surface of crystal 1. To compensate, we assumed a mask on the back surface of crystal 1 which lead to scaling the measured reflectance and transmittance up by a factor of 1.4 in the interval 1500–10000 cm^{-1}, thus explaining the difference between Fig. 3 and Fig. 4. The scaled reflectance and transmittance yielded a single bounce reflectance which agreed well with the measured bulk reflectance in regions where crystal 1 did not transmit, as shown in Fig. 4.

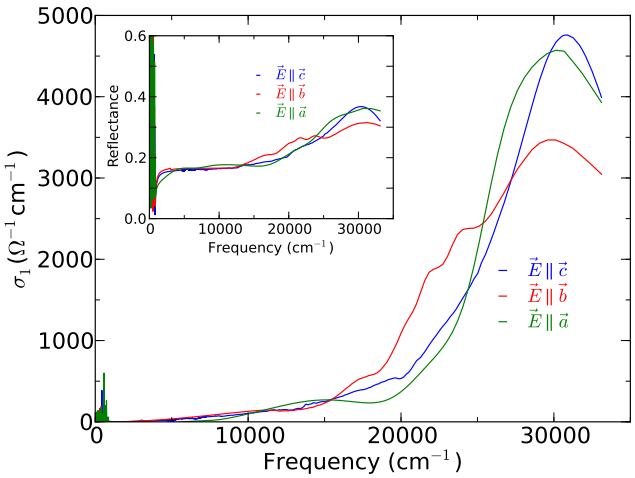

FIG. 5. (Color online) The optical conductivity in the frequency interval 30–33000 cm^{-1} at 300 K. The inset shows the 300 K broadband reflectance out to 33000 cm^{-1} from which the optical conductivity was extracted via Kramers-Kronig relations.

Kramers-Kronig analysis can be used to estimate the real and imaginary parts of the dielectric function from the bulk reflectance $R(\omega)$.[22] Before calculating the Kramers-Kronig integral, the low frequency data (0.1–30 cm^{-1}) were extrapolated using parameters from the complex dielectric function model described in Sec. III E. At high frequencies (8×10^4–2.5×10^8 cm^{-1}) the reflectance was approximated from known x-ray scattering functions of the constituent atoms. The gap between our highest measurable frequency and the x-ray reflectance data was bridged with a Lorentz oscillator at 60000 cm^{-1}. Subsequently, the phase shift on reflection was obtained via Kramers-Kronig analysis, and the optical properties were calculated from the reflectance and phase.

Figure 5 displays the optical conductivity parallel to the three crystallographic axes in the frequency interval 30–33000 cm^{-1}. The strong anisotropy observed in the far infrared persists at high frequencies resulting in three distinct absorption edges. The inset of Fig. 5 shows the 300 K reflectance up to 33000 cm^{-1} parallel to the a, b, and c axes.

The differences in energy of the high frequency transmission edge measured parallel to the b and c axes agree with the anisotropy seen in the optical conductivity at high frequencies (Fig. 5).

E. Oscillator-model fits

The measured reflectance was fit with a Drude-Lorentz model to obtain a second estimate of the complex dielectric function in the infrared range. The model assigns a Lorentzian oscillator to each distinguishable phonon in the spectrum plus a high frequency permittivity, ϵ_∞, to address the contribution of electronic excitations. The model has the following mathematical form:

$$\epsilon = \sum_{j=1}^{\infty} \frac{S_j \omega_j^2}{{\omega_j}^2 - \omega^2 - i\omega\gamma_j} + \epsilon_\infty \quad , \tag{1}$$

where S_j, ω_j, and γ_j signify the oscillator strength, center frequency, and the full width at half max (FWHM) of the jth Lorentzian oscillator. The Drude-Lorentz complex dielectric function is used to calculate the reflectivity, which is compared to the original measured quantity in Fig. 6. Similar qualities of fits were obtained for all other temperatures and polarizations.

IV. DISCUSSION

A. Group theory and lattice dynamics

Due to the lack of anomalies upon cooling below 10.6 K, we turn our focus to the highly anisotropic far-infrared excitation spectrum. The number of phonon modes expected in $FeTe_2O_5Br$ can be found by group-theory analysis. Using the SMODES program,[23] we arrive at the following distribution of modes:

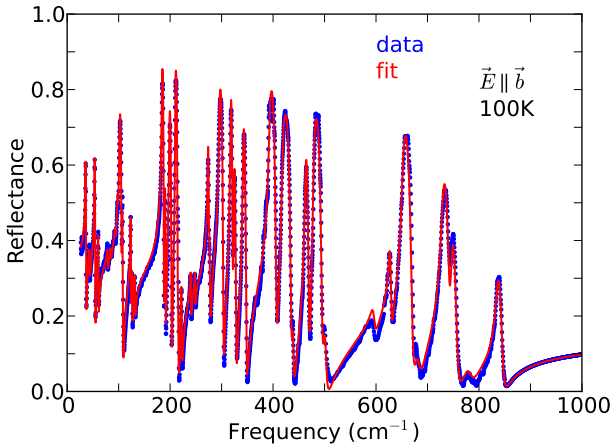

FIG. 6. (Color online) Experimental reflectance (blue points) and calculated reflectance (red line) from the Drude-Lorentz model of the $FeTe_2O_5Br$ 100 K b axis dielectric function.

TABLE I. Oscillator parameters for experimentally observed phonons along the a axis (at 20 K). The motions of atoms associated with groups of phonons have been assigned when the pattern was apparent. The atoms are listed in descending order of their calculated net atomic displacement.

j	Osc Str S_j	Ctr Freq ω_j (cm^{-1})	FWHM γ_j (cm^{-1})	Degenerate j in c	Atoms
1	0.207	45.5	2.0	1	Br
2	1.320	79.6	2.1	5	-
3	0.356	88.4	1.1	6	Br,Te,O,Fe
4	0.042	98.1	1.0	8	Br,Te,O,Fe
5	0.056	107.5	2.1	9	Br,Te,O,Fe
6	0.048	137.1	1.9	12	Br,Te,O,Fe
7	0.015	157.6	1.6	14	Te,Br,O,Fe
8	0.023	166.0	2.2	15	Te,Br,O,Fe
9	0.354	184.9	1.3	16	Te,O,Fe
10	0.519	194.3	2.4	17	Te,O,Fe
11	0.159	211.7	2.0		Te,O,Fe
12	0.007	236.4	4.9	22	-
13	0.084	247.8	1.7	23	-
14	0.009	256.5	4.0	24	-
15	0.169	291.9	1.8	27	Fe,O,Te
16	0.030	302.8	3.4		Fe,O,Te
17	0.033	321.6	3.6	28	Fe,O,Te
18	0.006	328.0	2.4		Fe,O,Te
19	0.003	348.5	2.0	29	Fe,O,Te
20	0.102	370.0	2.5		-
21	0.008	387.1	2.6		-
22	0.030	401.3	4.1		-
23	0.005	418.6	4.0		-
24	0.005	426.2	2.6	30	-
25	0.090	435.0	3.9	31	-
26	0.119	463.6	5.4	32	O,Fe,Te
27	0.004	481.0	1.4		O,Fe,Te
28	0.029	493.2	4.9	33	O,Fe,Te
29	0.350	575.3	7.5	35	O,Fe
30	0.203	666.1	8.0	37	O,Fe
31	0.257	730.5	13.9		O,Fe
32	0.018	784.0	9.2	42	-

TABLE II. Oscillator parameters for experimentally observed phonons along the c axis (at 20 K). The motions of atoms associated with groups of phonons have been assigned when the pattern was apparent. The atoms are listed in descending order of their calculated net atomic displacement.

j	Osc Str S_j	Ctr Freq ω_j (cm^{-1})	FWHM γ_j (cm^{-1})	Degenerate j in a	Atoms
1	4.275	46.7	0.2	1	Br
2	1.335	53.9	0.5		Br
3	0.951	65.8	1.0		-
4	0.216	71.7	0.8		-
5	0.435	81.2	0.9	2	-
6	0.205	89.3	0.9	3	Br,Te,O,Fe
7	0.061	97.0	0.8		Br,Te,O,Fe
8	0.130	99.0	1.1	4	Br,Te,O,Fe
9	0.533	109.2	0.8	5	Br,Te,O,Fe
10	0.294	112.8	1.0		Br,Te,O,Fe
11	0.369	128.5	0.8		Br,Te,O,Fe
12	0.127	135.4	0.9	6	Br,Te,O,Fe
13	0.411	140.6	0.9		-
14	0.857	157.0	0.5	7	Te,Br,O,Fe
15	0.107	166.8	1.0	8	Te,Br,O,Fe
16	0.212	184.5	0.6	9	Te,O,Fe
17	0.039	194.8	1.2	10	Te,O,Fe
18	0.066	204.0	1.4		-
19	0.014	206.3	1.1		-
20	0.085	221.7	1.1		-
21	0.101	225.4	0.9		-
22	0.065	232.6	1.0	12	-
23	0.107	248.0	1.5	13	-
24	0.291	254.2	0.6	14	-
25	0.239	274.4	1.1		-
26	0.195	284.9	1.2		-
27	0.633	294.8	1.4	15	Fe,O,Te
28	0.138	319.0	1.9	17	Fe,O,Te
29	0.173	349.0	2.2	19	Fe,O,Te
30	0.514	426.7	2.4	24	-
31	1.562	437.0	2.3	25	-
32	0.088	459.3	3.4	26	O,Fe,Te
33	0.006	488.5	4.3	28	O,Fe,Te
34	0.067	509.6	9.6		O,Fe,Te
35	0.260	573.5	5.6	29	O,Fe
36	0.096	626.7	5.2		O,Fe
37	0.015	662.0	3.2	30	O,Fe
38	0.061	672.0	5.7		O,Fe
39	0.182	693.5	8.9		O,Fe
40	0.172	707.4	5.2		O,Fe
41	0.101	749.8	9.4		-
42	0.014	780.4	6.6	32	-
43	0.033	814.7	6.9		-

$$\Gamma^{optical} = 54A_g^{(R)} + 54B_g^{(R)} + 53A_u^{(IR)} + 52B_u^{(IR)} \quad , \tag{2}$$

where (R) and (IR) denote Raman active and infrared active modes respectively. The $53A_u$ modes are expected to lie along the unique b axis of the monoclinic system and one should theoretically be able to resolve all 53 modes. However, the merging of weaker modes near stronger modes can hinder this count. The $52B_u$ modes are expected to lie in the ac plane, and presumably each mode can possess a distinct set of principal axes within the ac plane. We cannot accurately count the B_u modes because a pristine ac plane was not available for measurement. We can however discuss the phonon response with light polarized parallel to both the a and c axes of the crystal. To assist our analysis of the phonon spectra we employed lattice dynamical calculations to determine the relative resonance frequency, mode intensity, as well as displacement pattern for the 105 IR-active modes. The calculations, which

TABLE III. Oscillator parameters for experimentally observed phonons along the b principal axis (at 20 K). The motions of atoms associated with groups of phonons have been assigned when the pattern was apparent. The atoms are listed in descending order of their calculated net atomic displacement.

j	Osc Str S_j	Ctr Freq ω_j (cm^{-1})	FWHM γ_j (cm^{-1})	Atoms
1	1.388	35.7	0.8	Br
2	0.330	43.5	1.4	Br
3	0.899	53.2	0.8	-
4	0.289	60.5	0.9	Br,Te,O,Fe
5	0.119	79.1	1.3	Br,Te,O,Fe
6	0.075	85.0	1.2	Br,Te,O,Fe
7	0.052	91.2	1.0	Br,Te,O,Fe
8	0.138	93.3	1.3	-
9	0.259	98.0	0.9	-
10	1.359	102.0	1.1	-
11	0.073	106.9	0.7	-
12	0.170	123.7	0.7	Te,Br,O,Fe
13	0.092	126.3	0.9	Te,Br,O,Fe
14	0.074	131.4	1.1	Te,Br,O,Fe
15	1.066	184.2	1.0	Te,O,Fe
16	0.128	190.2	0.7	Te,O,Fe
17	0.491	198.6	0.8	Te,O,Fe
18	0.440	210.0	0.3	-
19	0.023	215.3	1.3	-
20	0.053	222.0	1.1	-
21	0.058	240.1	1.3	-
22	0.028	249.0	0.9	-
23	0.274	273.9	0.9	Fe,O,Te
24	0.102	275.8	1.4	Fe,O,Te
25	0.661	295.5	1.3	Fe,O,Te
26	0.366	317.6	1.9	Fe,O,Te
27	0.101	324.3	1.5	Fe,O,Te
28	0.261	341.7	1.2	Fe,O,Te
29	0.808	393.7	2.6	Fe,O,Te
30	0.371	418.0	4.1	-
31	0.009	437.7	3.5	-
32	0.209	463.1	3.9	O,Fe,Te
33	0.173	478.0	3.3	O,Fe,Te
34	0.012	499.0	4.6	-
35	0.009	508.3	1.2	-
36	0.047	595.3	6.9	O,Fe
37	0.080	626.6	3.6	O,Fe
38	0.323	652.0	4.9	O,Fe
39	0.018	682.1	8.2	O,Fe
40	0.217	728.1	7.8	O,Fe
41	0.027	746.2	7.4	-
42	0.031	779.9	23.5	-
43	0.071	836.0	9.6	-

utilized the structure and valence as reported by Becker *et al.*,[14] were based on a real-space summation of screened Coulomb interactions involving a spherical cut-off boundary.[24] The following two sections describe the method used to compare the observed and calculated spectrum for the A_u and B_u modes respectively.

B. 52B_u modes

All 52B_u modes predicted lie in the ac plane and should possess a finite intensity along both measured polarizations in this plane unless the direction of the induced dipole moment for a particular vibration is parallel to either the a or c axis. (Small angular deviations from the parallel case may be hard to detect.) The $FeTe_2O_5Br$ crystals measured lacked an optically flat ac plane; however, measurements with light polarized parallel to both the a and c axes are

reported. The phonon spectra parallel to the a and c axes are summarized in Table I and Table II respectively. The modes observed are grouped into one of two categories: modes observed are present exclusively in either the a or c spectra, or modes are observed in both the a and c spectra. For the latter possibility, we have identified and subsequently attempted to correlate phonon modes arising from the same physical vibrations that are present in both the a and c spectra. The modes were correlated using the following methodology: modes were grouped together if they were observed in the same small frequency interval (on the order of a typical linewidth) of one another in the two spectra. Next, we compared the experimental linewidths of the grouped modes to ensure that they would overlap if plotted side-by-side. As a final criterion, we compared the displacement patterns generated by our calculation to make sure they were in good agreement as to which excitations corresponded to the same physical vibrations. The correlation results are detailed in the columns titled "degenerate" in Table I and Table II. It is worthwhile noting that the modes observed simultaneously in both the a and c spectra may either induce dipole moments that are at an arbitrary angle between the a and c axes, or result from vibrations that are two-dimensional in nature. Angular dependent measurements in the ac plane are needed to clarify the aforementioned ambiguity. The oscillator strengths reported in Table I and Table II were obtained by fitting the reflectance spectra with a Lorentz oscillator model; however, the reported oscillator strengths for the modes classified as degenerate may only represent a projection of the true oscillator strength along the respective axis. Apropos the reported oscillator strengths of any two correlated modes that vary by at least an order of magnitude, one can make a conjecture as to which axis (a or c) the true polarization of the modes lies closest.

C. 53A_u modes

Counting the experimentally observed A_u modes is straightforward; we observe 43 of the 53 predicted modes along this direction. We believe that 10 modes were not observed as a result of weaker modes being buried within stronger modes and merging together in the spectrum. In the optical conductivity, all single-phonon excitations should be represented by symmetric Lorentzian oscillators. Figure 7 left panel depicts a slightly asymmetric Lorentzian oscillator with a resonance frequency of 85 cm^{-1}. Our attempt to fit the resonance at 85 cm^{-1} with a symmetric Lorentzian oscillator yields unaccounted for spectral weight on the high frequency side of the resonance. A symmetric Lorentzian oscillator centered at 79 cm^{-1} and corresponding fit are also included as a reference. (Note that the additional spectral weight between the resonances at 75 cm^{-1} and 85 cm^{-1} is attributed to absorption between the bands and therefore not to be mistaken for a lattice vibration). We suspect that this asymmetric shoulder is due to a weak buried mode that is not fully resolved. To further support our interpretation of buried modes, the right panel of Fig. 7 depicts the appearance of a once buried mode (∼276 cm^{-1}) upon cooling. The Lorentz oscillator parameters of the 52B_u modes at 20 K are found in Table III.

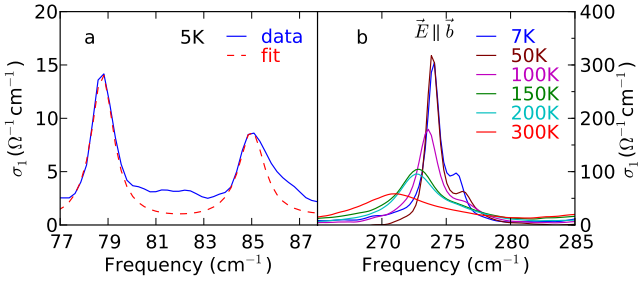

FIG. 7. (Color online) The left panel (a) shows unaccounted for spectral weight on the high frequency side of the asymmetric oscillator at 85 cm^{-1} along with a fit to a symmetric oscillator (79 cm^{-1}). We suspect the asymmetric shoulder is the result of a buried mode. The right panel (b) depicts the appearance of a once buried mode (∼276 cm^{-1}) upon cooling.

D. Temperature-Dependent Phonon Parameters

$FeTe_2O_5Br$ exhibits no clear infrared signature of spatial inversion symmetry breaking below T_N (mandated by the onset of ferroelectricity). This puzzling lack of a symmetry-lowering signature, such as an extra phonon, is actually common to many multiferroic materials. However, the frequencies of infrared phonons have been reported to become

renormalized below the magnetic transition in a number of multiferroics.[25] The mechanism of the aforementioned renormalization of phonon frequencies is likely an effect caused by magnetostriction.[26,27] We have thoroughly investigated the phonon spectra above and below T_N and have found no signature of a renormalization of the parameters extracted from our fits. The center frequency and linewidth of three select phonons parameters along the b axis are presented in Fig. 8.

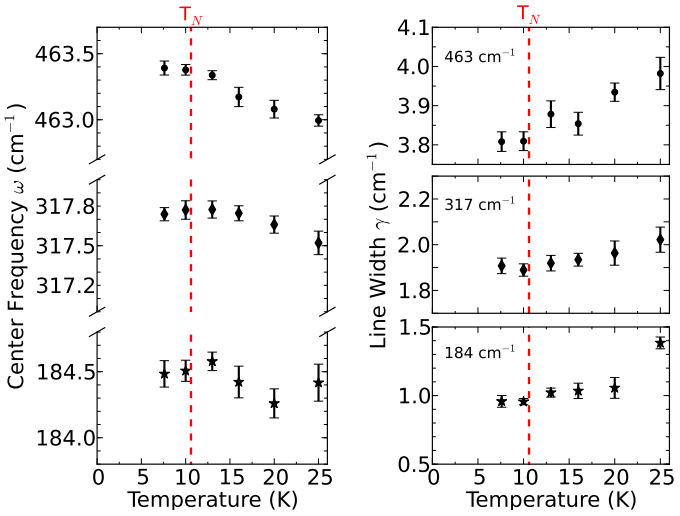

FIG. 8. (Color online) The center frequency and linewidth of three select phonon parameters along the b axis. No renormalization of the phonon parameters below T_N is observed within the error of determining their respective values.

E. Assignment of Modes

The assignment of a particular phonon observed in the experimental spectrum to its precise atomic displacement pattern cannot be made without sacrificing objective certainty because of the density of the phonon spectrum. Assignments to groups of modes, however, can be made through the displacement patterns generated by our lattice dynamical calculations. Using a simplified model of a phonon as a driven oscillator with resonant frequency inversely proportional to mass, we proceed to list the constituent atoms in the structure from heaviest to lightest: Te, Br, Fe, and O. Normally, the low frequency modes involve the heaviest atoms, but in the $FeTe_2O_5Br$ structure the Br atoms have a weak interaction with the other atoms and therefore are responsible for the lowest frequency phonons. At a certain frequency the motion of Br atoms will cease. Likewise, at a higher frequency the vibration of atoms involving Te will cease, leaving the motion of Fe and O to be expected in the highest frequency phonons. Accordingly, the phonon spectrum can be divided into three clusters that is reflected in Fig. 2 (namely, below 180 cm^{-1}, between 180 cm^{-1} and 530 cm^{-1}, and above 530 cm^{-1}). The clustering is also observed in the calculated spectrum via the displacement patterns produced, in terms of first the Br and subsequently the Te ceasing to vibrate. Within each cluster trends are to be noted on the following principle: atoms are listed corresponding to their net atomic displacement. This approach, in turn, has allowed us to identify another characteristic of atomic displacement within the three clusters. The atom of focus in a cluster (e.g., Br in the first cluster) has a net atomic displacement ever diminishing. Cessation does not arrive abruptly. The three clusters are profiled in each of Table I, Table II, and Table III.

Apropos the third cluster that focuses on Fe and O, an additional resource is provided by the familiar orthoferrite family of compounds because the FeO_6 octrahedral building block that is present in $FeTe_2O_5Br$ is itself a defining unit of the orthoferrite family. Given the abundant literature on vibrational assignments made to the FeO_6 octrahedral unit,[28,29] we are consequently able to map these well recognized assignments onto our experimental findings, thus corroborating both perspectives.

V. CONCLUSIONS

Far-infrared measurements on multiferroic single-crystal $FeTe_2O_5Br$ reveal no drastic anomalies in the excitation spectrum below the multiferroic ordering temperature. Nonetheless, a thorough inspection of the phonon spectra has

lead to the identification of 43 of the 53 predicted modes along the unique b axis. The absence of 10 modes along the b axis is presumably due to the merging of weaker modes near stronger modes in the dense excitation spectrum. Two orthogonal polarizations were measured in the ac plane; however, a full analysis of the $52B_u$ modes awaits a single crystal of $FeTe_2O_5Br$ with an optically flat ac surface.

The motions of individual atoms have been assigned to groups of phonons via the displacement patterns produced through our lattice dynamical calculation. The assignments divide the overall phonon spectrum into three clusters, which are characterized by an atom that is common to every vibration in that cluster. We observed that as frequency increases, vibrations involving the motion of Br atoms will progressively cease. Likewise, at higher frequencies the vibrations involving Te atoms will cease in the same manner, leaving the motion of Fe and O to be expected in the highest frequency phonons. Moreover, the particular atoms involved in a vibration are listed in descending order of net atomic displacement, which in turn makes clear a trend within each cluster (namely, the atom of focus in a particular cluster has a net atomic displacement ever diminishing).

It remains to compare our results to a recent infrared study by Pfuner *et al.*[13] on the similar $FeTe_2O_5Cl$ compound where an equal number of phonons were predicted. Our analysis of the phonon spectrum agrees with the infrared study of Pfuner *et al.* in that we also believe modes resonating at equivalent energy scales can overlap, preventing them from being resolved separately, but we differ on other issues. Pfuner *et al.* report a combined 38 modes along the b and c directions. We observe more modes along the unique b axis alone, as well as modes below 50 cm^{-1}, whereas the study by Pfuner *et al.* does not report measurements below this frequency.

We also observe drastically different and more strongly anisotropic high frequency optical properties. Pfuner *et al.*[13] report an absorption edge around 4,000 cm^{-1} in $FeTe_2O_5Cl$, where as we observe low absorption accompanied by substantial transmission through the $FeTe_2O_5Br$ crystal in this region. In speculating about the differences in high frequency optical properties of the two similar compounds, we point out that spurious changes of slope of the reflectance throughout the mid-infrared region, such as those resulting from the contribution of back surface reflection (black line in Fig. 4), can drastically change the Kramers-Kronig-derived optical properties.

Transmission measurements as well as reflectance along a were not reported in the study by Pfuner *et al.*. Similar to the $FeTe_2O_5Br$ system reported here, the $FeTe_2O_5Cl$ system also showed no response to magnetic fields above or below the magnetic ordering temperature.

ACKNOWLEDGMENTS

The authors thank M. Pregelj for providing low-temperature crystallographic information files. This work was supported by DOE through grant DE-FG02-02ER45984 at UF and DE-AC02-98CH10886 at the NSLS.

[1] Y. Yamasaki, H. Sagayama, T. Goto, M. Matsuura, K. Hirota, T. Arima, and Y. Tokura, Phys. Rev. Lett. **98**, 147204 (2007).
[2] Y. Bodenthin, U. Staub, M. Garca-Fernndez, M. Janoschek, J. Schlappa, E. I. Golovenchits, V. A. Sanina, and S. G. Lushnikov Phys. Rev. Lett. **100**, 027201 (2008).
[3] V. S. Zapf, M. Kenzelmann, F. Wolff-Fabris, F. Balakirev, and Y. Chen, Phys. Rev. B **82**, 060402 (2010).
[4] T. Goto, T. Kimura, G. Lawes, A. P. Ramirez, and Y. Tokura, Phys. Rev. Lett. **92**, 257201 (2004).
[5] S.-W. Cheong and M. Mostovoy, Nat. Mater. **6**, 13 (2007).
[6] T. Kimura, T. Goto, H. Shintani, K. Ishizaka, T. Arima, and Y. Tokura, Nature (London) **426**, 55 (2003).
[7] M. Kenzelmann, G. Lawes, A. B. Harris, G. Gasparovic, C. Broholm, A. P. Ramirez, G. A. Jorge, M. Jamie, S. Park, Q. Huang, A. Ya. Shapiro, and L. A. Demianets, Phys. Rev. Lett. **98**, 267205 (2007).
[8] Y. Yamasaki, S. Miyasaka, Y. Kaneko, J.-P. He, T. Arima, and Y. Tokura, Phys. Rev. Lett. **96**, 207204 (2006).
[9] I. A. Sergienko, C. Sen, and E. Dagotto, Phys. Rev. Lett. **97**, 227204 (2006).
[10] S. Picozzi, K. Yamauchi, B. Sanyal, I. A. Sergienko, and E. Dagotto, Phys. Rev. Lett. **99**, 227201 (2007).
[11] P. G. Radaelli, C. Vecchini, L. C. Chapon, P. J. Brown, S. Park, and S.-W. Cheong, Phys. Rev. B **79**, 020404 (2009).
[12] M. Pregelj, A. Zorko, O. Zaharko, Z. Kutnjak, M. Jagodic, Z. Jaglicic, H. Berger, M. de Souza, C. Balz, M. Lang, and D. Arcon, Phys. Rev. B **82**, 144438 (2010).
[13] F. Pfuner, L. Degiorgi, H. Berger, and L. Forro, J. Phys.: Condens. Matter **21**, 375401 (2009).
[14] R. Becker, M. Johnsson, R. K. Kremer, H.-H. Klauss, and P. Lemmens, J. Am. Chem. Soc. **128**, 15469 (2006).
[15] M. Pregelj, O. Zaharko, A. Zorko, Z. Kutnjak, P. Jeglic, P. J. Brown, M. Jagodic, Z. Jaglicic, H. Berger, and D. Arcon, Phys. Rev. Lett. **103**, 147202 (2009).
[16] O. Zaharko, M. Pregelj, D. Arcon, P. J. Brown, D. Chernyshov, U. Stuhr, and H. Berger, J. Phys.: Conf. Ser. **211**, 012002 (2010).
[17] X Xi, J. Hwang, C. Martin, D. B. Tanner, and G. L. Carr, Phys. Rev. Lett. **105**, 257006 (2010).

[18] A. B. Kuz'menko, E. A. Tishchenko, and V. G. Orlov, J. Phys.: Condens. Matter **8**, 6199 (1996).
[19] M. Born and E. Wolf, *Principles of optics* (Cambridge University Press, United Kingdom, 1999).
[20] M. Pregelj, H. O. Jeschke, H. Feldner, R. Valentí, A. Honecker, T. Saha-Dasgupta, H. Das, S. Yoshii, T. Morioka, H. Norjiri, H. Berger, A. Zorko, O. Zaharko, and D. Arčon, Phys. Rev. B **86**, 054402 (2012).
[21] A. Zibold, H. L. Liu, S. W. Moore, J. M. Graybeal, and D. B. Tanner, Phys. Rev. B **53**, 11734 (1996).
[22] F. Wooten, *Optical Properties of Solids* (Academic Press, New York, 1972).
[23] H. T. Stokes and D. M. Hatch, 1999 SMODES, www.physics.byu.edu/stokesh/isotropy.html.
[24] D. Wolf, P. Keblinski, S. R. Phillpot, and J. Eggebrecht, J. Phys. Chem. **110**, 8254 (1999).
[25] R. Schleck, R. L. Moreira, H. Sakata, and R. P. S. M. Lobo, Phys. Rev. B **82**, 144309 (2010).
[26] T. Rudolf, Ch. Kant, F. Mayr, and A. Loidl, Phys. Rev. B **77**, 024421 (2008).
[27] R. Schleck, Y. Nahas, R. P. M. S. Lobo, J. Varignon, M. B. Lepetit, C. S. Nelson, and R. L. Moreira, Phys. Rev. B **82**, 054412 (2010).
[28] P. Hermet, M. Goffinet, J. Kreisel, and Ph. Ghosez, Phys. Rev. B **75**, 220102 (2007).
[29] V.L Mathe, K.K Patankar, R.N Patil, C.D Lokhande, J. Magn. Magn. Mater. **270**, 380 (2004).